



1 **Characterization of the Atlantic Water and Levantine Intermediate**
2 **Water in the Mediterranean Sea using Argo Float Data**

3

4 Fedele Giusy^{1,*}, Mauri Elena¹, Notarstefano Giulio¹ and Poulain Pierre Marie¹

5

6 (1) National Institute of Oceanography and Applied Geophysics, OGS, 34010 Sgonico (TS), Italy

7 * Corresponding author (gfedele@inogs.it)

8 The Atlantic Water (AW) and Levantine Intermediate Water (LIW) are important water
9 masses that play a crucial role in the internal variability of the Mediterranean thermohaline
10 circulation. In particular, their variability and interaction, along with other water masses that
11 characterize the Mediterranean basin, such as the Western Mediterranean Deep Water (WMDW),
12 contribute to modify the Mediterranean Outflow through the Gibraltar Strait and hence may
13 influence the stability of the global thermohaline circulation.

14 This work aims to characterize the AW and LIW in the Mediterranean Sea, taking advantage
15 of the large observational dataset provided by Argo floats from 2001 to 2019. Using different
16 diagnostics, the AW and LIW were identified, highlighting the inter-basin variability and the
17 strong zonal gradient that characterize the two water masses in this marginal sea. Their temporal
18 variability was also investigated focusing on trends and spectral features which constitute an
19 important starting point to understand the mechanisms that are behind their variability. A clear
20 salinification and warming trend have characterized the AW and LIW in the last two decades
21 (~ 0.007 and 0.008 yr^{-1} ; 0.018 and $0.007 \text{ }^\circ\text{C yr}^{-1}$, respectively). The salinity and temperature trends
22 found at subbasin scale are in good agreement with previous results. The strongest trends are
23 found in the Adriatic basin in both the AW and LIW properties. A subbasin dependent spectral
24 variability emerges in the AW and LIW salinity timeseries with peaks between 2 and 10 years.

25 **Keywords:** Argo, Atlantic Water, Interannual variability, Inter-basin variability, Levantine
26 Intermediate Water, Mediterranean Sea, Trends



27 **Acknowledgments**

28 This research was funded by the Italian Ministry of University and Research as part of the Argo-
29 Italy program.

30

31 **1 Introduction**

32 The Atlantic Water (AW) and Levantine Intermediate Water (LIW) play a central role in the
33 internal variability of the Mediterranean thermohaline circulation, contributing to the dense water
34 formation in this enclosed basin (Tsimplis et al., 2006). The variability and interaction of these
35 two water masses modulate the Mediterranean outflow through the Gibraltar Strait, which plays
36 an important role on the North Atlantic oceanic variability, and in turn to the stability of the global
37 thermohaline circulation (e.g., Rahmstorf, 2006; Hernandez-Molina et al., 2014). Therefore, from
38 a climatic point of view, it is relevant to characterize their main properties and monitor their
39 variability, which are the main purpose of this paper.

40 Flowing in the Mediterranean Sea through the Gibraltar strait, the AW is less dense than the
41 surrounding water masses and therefore it populates most of the Mediterranean surface layer. Its
42 path is mainly driven by the Coriolis effect and by the complex topography that characterizes this
43 region (Millot and Taupier-Letage 2005).

44 The LIW is the most voluminous water mass produced in the Mediterranean Sea (e.g., Skliris
45 2014; Lascaratos et al., 1993), and the saltiest water formed with a relatively high temperature at
46 intermediate depths. It is formed in the Levantine subbasin, after which it is named, where one of
47 the main formation sites is the Rhodes Gyre (e.g., Tsimplis et al., 2006; Kubin et al., 2019). The
48 LIW strongly influences the thermohaline circulation, flowing at intermediate depths and then
49 passing over the sills, exiting the Gibraltar Strait and modifying the Atlantic circulation (Millot
50 and Taupier-Letage, 2005).

51 Several studies have been devoted to the analysis of the AW and LIW main features and
52 variability, taking advantage of different indicators to identify and track these two water masses
53 in the Mediterranean Sea. Among them, the AW and the LIW are usually referred to the minimum



54 and maximum salinity in the surface and intermediate layers of the water column, respectively
55 (e.g., Millot and Taupier-Letage 2005; Bergamasco and Malanotte-Rizzoli, 2010; Mauri et al.,
56 2019; Kokkini et al., 2019). However, different approaches can also be found in the literature. In
57 particular Millot (2014) associated the LIW to the maximum of the potential temperature vertical
58 gradient found in an intermediate water layer, while Bosse et al. (2015) identified the LIW in the
59 northwestern Mediterranean Sea with the maximum salinity value found between two potential
60 density values ($\sigma_{\theta} = [29.03 - 29.10] \frac{kg}{m^3}$), encompassing both temperature and salinity maxima
61 characterizing the LIW layer. The main findings related to the hydrological properties of these
62 two water masses are summarized below.

63 The AW enters in the Mediterranean Sea through the Gibraltar Strait, occupying the upper 200
64 m of depth with potential density, temperature and salinity annual mean values: $\sigma_{\theta} \cong$
65 $[26.5 - 27] \frac{kg}{m^3}$, $T \cong [14 - 16]^{\circ}C$, $S \cong [36.0 - 36.5]$ respectively. The AW flowing at the
66 surface, continuously interacts with the atmosphere and is subject to evaporation and mixing with
67 the underlying water masses. Flowing eastward, it becomes denser and the minimum salinity core
68 sinks. Therefore, it can be capped by the surface mixed layer and less influenced by air-sea
69 interactions. Its properties and variability are also modified by the local eddies and by the river
70 discharges in the coastal regions. These mechanisms shape the AW, leading to an increase of
71 salinity from about 36.25 in the Gibraltar Strait to values around 39.2 in the Levantine Sea (e.g.,
72 Bergamasco and Malanotte-Rizzoli, 2010; Hayes et al., 2019). These values highlight strong AW
73 temperature and salinity gradients between the Western Mediterranean (WMED) and the Eastern
74 Mediterranean (EMED).

75 The properties of the LIW core in the WMED are commonly referred to the following ranges
76 of potential density, temperature, salinity and depth, respectively: $\sigma_{\theta} = [29 - 29.10] \frac{kg}{m^3}$, $T =$
77 $[13 - 14.2]^{\circ}C$, $S = [38.4 - 38.8]$, $D = [200 - 600]m$ (e.g. Millot, 2013; Hayes et al., 2019);
78 while in the EMED these properties span over different values: $\sigma_{\theta} = [28.85 - 29.15] \frac{kg}{m^3}$, $T =$
79 $[14.6 - 16.4]^{\circ}C$, $S = [38.85 - 39.15]$, $D = [150 - 400]m$ (e.g. Lascaratos et al., 1993; Hayes
80 et al., 2019). Therefore, moving westward, T and S decrease and the LIW sinks.



81 These studies provide a general view of the AW and LIW properties in the Mediterranean Sea,
82 highlighting a strong inter-basin variability of these water masses along their paths, which in turn
83 influences their temporal changes.

84 An example is given by a recent paper by Kassis and Korres (2020), which provides a detailed
85 view of the EMED hydrographic properties for the period 2004–2017 taking advantage of Argo
86 data. Exploring the water column from the surface down to 1500 m in seven different regions of
87 the EMED, they revealed a high inter-annual variability of the stored heat and salt over this region.

88 In this study, following a similar approach, we investigate the AW and LIW properties,
89 isolating their main characteristics and variability from the surrounding water masses, taking
90 advantage of several diagnostics discussed in section 2.2. Our work aims to provide a more
91 detailed view of the AW and LIW thermohaline properties over the last two-decades in most of
92 the Mediterranean Sea, investigating these two water masses through a subbasin approach, which
93 aims to emphasize how the processes that take place in each subbasin shape the water masses
94 properties. Their temporal variability is also studied, discussing the relative trends and spectral
95 features, which constitute an important starting point to understand the mechanisms that are
96 behind their variability.

97 In the frame of climate change studies, it is important to estimate possible impacts of AW and
98 LIW changes on the Mediterranean Climate, since this region is one of the most vulnerable
99 climate change hotspots (Giorgi 2006). In fact, changes in temperature and salinity can strongly
100 affect the marine system over the Mediterranean and related human activities.

101 Previous studies highlighted a clear salinification of the Mediterranean Sea over the past few
102 decades (e.g., Painter and Tsimplis 2003; Vargas -Yáñez et al., 2010; Schroeder et al., 2017;
103 Skliris et al., 2018) and a clear deep water warming trend after 1980s, which in literature is often
104 related to the Nile River damming and to the global warming (Vargas-Yáñez et al., 2010). Positive
105 temperature and salinity trends, oscillating between $[0.0016 \div 0.0091]$ °C/yr and $[0.0008 \div 0.001]$
106 yr⁻¹, respectively, are found in the deep layer (below ~700 meters) between 1950 to 2005 (e.g.,
107 Bethoux et al., 1990; Rohling and Bryden, 1992; Millot et al., 2006; Vargas-Yáñez et al., 2010;
108 Borghini et al., 2014).



109 This observed salinification and warming are also found at intermediate depths in several
110 studies (e.g., Zu et al., 2014; Schroeder et al., 2017; Skliris et al., 2018), with ranges that depend
111 on the region of investigation. A clear salinity positive trend between 150-600 m is found in the
112 Mediterranean Sea by Skliris et al. (2018), analyzing the MEDATLAS data from 1950 to 2002
113 ($\sim 0.007 \pm 0.004 \text{ yr}^{-1}$).

114 In contrast, heterogeneous temperature trends are found in the upper layer in different regions
115 (Painter and Tsimplis, 2003). This sensitivity of the trends to the area of interest, can be due to
116 several reasons, such as the changes in the large-scale atmospheric forcing of the Mediterranean
117 region, the river runoff which differ from one region to another, and to the data coverage over a
118 specific area (e.g., Painter and Tsimplis, 2003; Vargas -Yáñez et al., 2009; 2010). In this respect,
119 Vargas -Yáñez et al. (2009) highlighted that the scarcity of data makes trend estimations very
120 sensitive to the data postprocessing, comparing results from different studies dealing with the
121 same time period. Therefore, in order to reduce the uncertainty of the trend estimations, longer
122 and less sparse timeseries are needed.

123 In this respect, this work aims to provide an updated view of the temporal evolution and trends
124 of the AW and LIW, taking advantage of the large observational dataset provided by the MedArgo
125 Program (Poulain et al., 2007). It covers the water column from the surface down to ~ 2000 m
126 over the entire Mediterranean basin from 2001 to 2019. The Mediterranean Sea has been widely
127 studied through the deployment of hundreds of Argo profiling floats (Argo 2020) in the last two
128 decades as part of various national, European and international programs (Wong et al., 2021) and
129 with the participation of different institutions. For these reasons, this dataset constitutes an optimal
130 observational framework to investigate the AW and LIW properties.

131 The dataset and the methods used in this study are described in section 2, the results are
132 presented in section 3, where the inter-basin and inter-annual variabilities of the AW and LIW in
133 the Mediterranean Sea are shown. The main conclusions are drawn in section 4.

134

135 **2 Data and method**

136 **2.1 Data**



137 In this work the AW and LIW properties in the Mediterranean Sea are investigated taking
138 advantage of the Argo float dataset, which consists of more than thirty thousand *T-S* profiles for
139 the period 2001–2019. Since 2001, the number of observations is generally increasing, reaching
140 a peak of 4188 profiles in 2015, mainly thanks to the combined efforts of national and
141 international Argo initiatives. The deployments of most Argo floats in the Mediterranean were
142 coordinated by the MedArgo regional center (Poulain et al., 2007). In the Mediterranean, the
143 cycling period is usually reduced to 5 days, and the maximum profiling depth is mostly 700 or
144 2000 m (Poulain et al., 2007). The floats are equipped with Sea-Bird Conductivity-Temperature-
145 Depth (CTD) sensors (model SBE41CP; [www.seabird.com/sbe-41-argo-ctd/product-](http://www.seabird.com/sbe-41-argo-ctd/product-details?id=54627907875)
146 [details?id=54627907875](http://www.seabird.com/sbe-41-argo-ctd/product-details?id=54627907875)) with accuracies of $\pm 0.002^\circ\text{C}$, ± 0.002 and ± 2 dbar for temperature,
147 salinity and pressure, respectively. The data measured by the profilers are transmitted to satellites
148 (e.g., via the Iridium or Argos telemetry systems), then to ground receiving stations, processed
149 and real-time quality-controlled by the Argo Data Assembly Centres ([https://www.euro-](https://www.euro-argo.eu/Activities/Data-Management/Euro-Argo-Data-Centres)
150 [argo.eu/Activities/Data-Management/Euro-Argo-Data-Centres](https://www.euro-argo.eu/Activities/Data-Management/Euro-Argo-Data-Centres)), sent to the Global Data
151 Assembly Center and made available for free to users. The delayed-mode quality control applied
152 on pressure, temperature and salinity follows the guidelines described in the Argo Quality Control
153 Manual for CTD (e.g., Wong et al., 2021; Cabanes et al., 2016), in conjunction with other
154 procedures developed at regional level (Notarstefano and Poulain, 2008; Notarstefano and
155 Poulain, 2013) to check the salinity data and any potential drift of the conductivity sensor.

156 The analyses are performed in eight Mediterranean sub-basins following the climatological
157 areas defined by the EU/MEDARMEDATLAS II project
158 (<http://nettuno.ogs.trieste.it/medar/climatologies/medz.html>), emphasizing the processes that take
159 place in each sub-basin and modify the water mass properties. Fig. 1 shows the geographical
160 distribution of the Argo profiles from 2001 to 2019 in the eight sub-basins considered (Algerian,
161 Catalan, Ligurian, Tyrrhenian, Adriatic, Ionian, Cretan and Levantine). The Alboran, Aegean and
162 the Sicily Channel sub-basins are not analyzed in this work due to the scarcity of observations in
163 these areas.



164 Most sub-basins are well spatially covered, except for the Adriatic Sea, where the majority of
165 observations are concentrated in the South Adriatic Pit (SAP) and therefore it is important to keep
166 in mind that the results found for this region, are representative of the southern Adriatic Sea. The
167 SAP is an important deep water convection site in the Mediterranean Sea (e.g., Kokkini et al.,
168 2019; Mauri et al., 2021, Azzaro et al., 2012; Bensi et al., 2013) and therefore it is also considered
169 as a crucial area from a climatic perspective. The temporal distribution of the float data is different
170 in the various sub-basins: the longest time series are available in the Ionian, Cretan and Levantine
171 regions, with data from 2001 to 2019, followed by the Algerian, Ligurian and Tyrrhenian sub-
172 basins where data are available after 2003, and then by the Adriatic Sea with data only after 2009.
173 In this context, it is important to mention that the low density in space and time of the Argo
174 profiles induces uncertainties in the results, especially during the first years of the analyzed
175 period.

176

177 **2.2 Methods**

178 As discussed in the introduction, many indicators/characteristics have been adopted in
179 literature to track the AW and LIW in the Mediterranean Sea. Most of them consider, as best
180 indicator, the minimum/maximum salinity at surface/intermediate layer for the AW/LIW and
181 motivated us to follow a similar approach (e.g., Millot and Taupier-Letage, 2005; Bergamasco
182 and Malanotte-Rizzoli, 2010; Hayes et al., 2019; Lamer et al., 2019).

183 A preliminary step in this analysis was the post-processing: we first applied a time sub-
184 sampling on each profiler to obtain a more homogeneous dataset (Notarstefano and Poulain,
185 2009). This is applied to each float as follows: if the cycling period is 1 day or less, the profiles
186 are sub-sampled every 5 days; if the period is 2 or 3 days, they are sub-sampled every 6 days; and
187 if the period is 5 or 10 days, no subsampling is applied. Afterward, each profile was linearly
188 interpolated from the surface (0 m) to the bottom every 10 m to obtain comparable profiles; and
189 finally, a running filter with a 20 m window, was applied to the data along the depth axis, in order
190 to smooth any residual spike.



191 After the post-processing, we proceeded with the search of the minima/maxima salinity peaks
192 for the AW/LIW between 0-100/100-700 m for each profile. We define a peak as a data point that
193 is smaller/larger than its two neighboring samples for the AW/LIW, imposing a minimum
194 difference value of 0.01. If no peaks are found due to high vertical mixing, the profile is excluded.
195 The peak with the maximum prominence in the salinity field identifies the AW/LIW in each
196 profile and is used to identify the respective depth and temperature of the water mass core.
197 Moreover, if the minimum/maximum salinity is located at the profile endpoints between 0-
198 100/100-700 m, it is associated to the AW/LIW only if its closest value satisfies the minimum
199 difference condition.

200 The number of profiles counted in each subbasin therefore not only depends on the data
201 sampling over that region, but also on external processes acting on the layer of interest such as
202 the mixing activity due to eddies and/or air-sea interaction: the stronger is the mixing, the lower
203 is the number of profiles considered.

204 Once the AW and LIW core are identified in each profile from 2001 to 2019, the AW and LIW
205 timeseries were computed in each subbasin to analyze the low frequency variability (LFV) and
206 trends at interannual to decadal timescale over the available timeseries. In this respect, the high
207 frequency variability was filtered out, first by subtracting the mean seasonal cycle to the raw
208 timeseries, and then applying a median yearly average filter. This last step is needed since the
209 data are not homogeneous in time in every subbasin from 2001 to 2019, and therefore without it,
210 the seasonal variability can contaminate the estimation of the trends. The latter have been
211 computed using the linear least-squares method to fit a linear regression model to the data.

212 The AW and LIW inter-basin variabilities were analyzed taking advantage of the boxplot
213 approach applied to each parameter and region (Fig. 2). Inside each grey box, the black bold line
214 indicates the median, while the bottom and top edges of the box indicate the 25th and 75th
215 percentiles respectively, and the black dots show the mode of each distribution, which
216 corresponds to the maximum probability density function (PDF). The whiskers (black dashed line
217 out of the box) extend to the most extreme data points not considering the outliers at the 5%
218 significance level ($pvalue \leq 0.05$). In order to test the significance, the Student's t distribution



219 was applied to each hydrological parameter in every sub-basin (Kreyszig and Erwin 1970). The
220 null hypothesis (that states that the population is normally distributed) is rejected with a 5% level
221 of statistical significance. This method is also applied to the timeseries trends.

222 In section 3.1 we often refer to the range and skewness of the distributions, that are the
223 difference between the upper and lower limits and the measure of the symmetry of the
224 distributions, respectively (including only the 5% significance values).

225 After the timeseries post-processing, in order to provide a time-evolving map of the spectral
226 features in each subbasin for the AW and LIW hydrological properties, the continuous wavelet
227 transform (CWT; Grossman et al., 1990) was applied to the 1-year moving averaged time series.
228 The time series were also linearly interpolated in order to fill in small gaps. In this respect, to
229 evaluate the significance of the wavelet transform we took advantage of the Matlab ASToolbox
230 provided by Conraria and Soares (2011) and available at
231 <http://sites.google.com/site/aguiarconraria/joanasoares-wavelets>, based on Monte Carlo
232 simulations (Berkowitz and Kilian, 2000). Wavelet power spectra were estimated.

233

234 **3 Results and discussion**

235 In this section, the AW and LIW properties are investigated in the eight Mediterranean regions
236 before mentioned, focusing both on their spatial and temporal variability. The analysis of the
237 trends and spectral features are also shown.

238

239 **3.1 Inter-basin variability**

240 (i) AW

241 The hydrological properties of the AW core in eight sub-basins (Fig. 1) are shown in Figs. 2a,
242 b, c, providing a compact view of the AW inter-basin variability for each parameter using the
243 boxplot approach.

244 In the whole Mediterranean Sea, several profiles are ignored (Fig.2d) because the minimum
245 salinity peak is smoothed by the air-sea interaction and eddies especially during winter (here not
246 shown). About the 20-30% of the data in most of the subbasins is discarded, while this percentage



247 exceeds ~34% in the Levantine subbasins, where the AW core is strongly perturbed by internal
248 and external processes (Malanotte-Rizzoli et al., 2003). Despite the substantial quantity of
249 excluded profiles (Fig. 2d), we were able to identify in a robust way the AW core in the available
250 dataset, characterizing its main properties and variability.

251 Moving eastward, the AW salinity increases from ~36 to 39.5 (minimum and maximum
252 whiskers limits; Fig. 2a), since the surface salinity minimum is progressively smoothed by
253 horizontal mixing with surrounding saltier waters. In fact, as discussed by Font et al. (1998) the
254 AW minimum salinity is dependent on the different degrees of mixing due to its residence times.

255 In the Algerian sub-basin, the salinity range reaches the highest extension compared to the
256 other regions, probably due to the large baroclinic instability that produces high mesoscale
257 variability in the surface layer and horizontal mixing by strong eddies (Demirov and Pinardi
258 2007).

259 The AW salinity range is smaller in the Catalan, Ligurian and Tyrrhenian Seas, where similar
260 distributions are found both in terms of range and skewness (which is close to zero): the main
261 mode and the median have salinity of ~38. In the Adriatic Sea the distribution is probably skewed
262 toward higher values because a clear positive salinity trend is found (Fig. 3; Lipizer et al., 2014).
263 In the Adriatic, Ionian and Cretan Seas, the range is higher than the surrounding sub-basins: in
264 the Adriatic and Ionian Sea this could be associated to the Bimodal Oscillation System (BiOS),
265 and then to the reversal of the North Ionian Gyre (Rubino et al., 2020), while in the Cretan Sea
266 we speculate that it is caused by the sinking of the AW during winter. This is in agreement with
267 Schroeder (2019), where it is shown that in the Cretan Sea, the strong wind-induced evaporation
268 and heat loss during winter lead the AW transformation into salty and warm Cretan Intermediate
269 Water. The depths reached in the Cretan basin (Fig. 2c) seem to confirm this hypothesis.

270 The AW temperature is highly variable, ranging between ~5 and ~30 °C, with a wider range
271 in the Catalan and Adriatic regions (Fig. 2b), possibly due to the higher seasonal sea surface
272 temperature variability over these sub-basins (Shaltout and Omstedt 2014). The lowest
273 temperatures detected can be related to the freshwater fluxes in these regions. In this respect, an
274 episode that can be relevant for the AW distribution in the Adriatic Sea is the large river runoff



275 observed in 2014 by Kokkini et al. (2019), which caused a saline stratification for more than a
276 year. This episode is also captured by our analyses (Fig. 3). As observed for the AW salinity
277 mode, even the temperature mode shift toward higher values moving eastward in agreement with
278 the literature (Bergamasco and Malanotte-Rizzoli 2010). In the Algerian basin the AW
279 temperature mode is higher than it is in the Catalan subbasin: this can be due to the influence of
280 freshwater fluxes in the Catalan region and led by the high eddy activity over the Algerian region
281 (Escudier et al., 2016) led by the strong baroclinic instability already discussed for the salinity
282 field (Demirov and Pinardi 2007).

283 The depths of the AW core oscillate between 0 and 90 m with the main mode sinking eastward
284 (Fig. 2c). The distributions are all skewed toward lower depths, with the maximum PDF near
285 surface and a median shifting from 0 to 45 m moving eastward, indicating a clear sinking of the
286 AW along its pathway.

287

288 (ii) LIW

289 In this section, the main hydrological properties of the LIW are analyzed in each sub-basin.
290 Comparing the percentages of the number of detected LIW cores related to the total profiles (Fig.
291 2h), it is evident that less convection occurs at these depths in most of the Mediterranean Sea, and
292 therefore less profiles are excluded compared to the AW. However more profiles are rejected in
293 the Adriatic and Levantine Seas, because strong mixing processes tend to smooth the LIW core
294 in the intermediate layer. In fact, as already mentioned, the SAP is an important deep water
295 convection site (Azzaro et al., 2012; Bensi et al., 2013; Kokkini et al., 2019), while the Levantine
296 basin is the region where the LIW formation occurs.

297 In the other sub-basins, more than the ~80% of profiles is considered, suggesting that
298 identifying the LIW is much easier than the AW, which is highly perturbed by external forcings.

299 Flowing away from the region of formation, the LIW interacts with the surrounding water
300 masses and becomes less salty; the salinity gradually drops from ~39.2 to ~38.4 from the
301 Levantine to the Ligurian subbasin and then the trend becomes almost flat in the Catalan and
302 Algerian regions (Fig.2e). The distributions are highly symmetric around the median and the



303 variability decreases flowing westward maybe because the LIW becomes deeper, sinking from
304 ~100 to ~650 m (Fig. 2g). The highest salinity is reached in the Cretan basin, where the formation
305 of salty and warm Cretan Intermediate Water, caused by strong wind-induced evaporation and
306 heat loss during winter, influences the LIW properties and detection (Schroeder, 2019).

307 The LIW temperature decreases westward from ~18 to ~12.8 °C. The range is higher in the
308 EMED as also found for salinity, suggesting that over this region, the intrusion of warmer and
309 saltier surface waters due to convective processes characterizes the LIW formation (Fig. 2f;
310 Schroeder, 2019).

311 The sinking of the LIW flowing westward is shown in Fig. 2g, dropping from about 100 to
312 650 m (maximum whiskers values). The distributions tend to be symmetric in most of the
313 Mediterranean Sea, except for the Adriatic Sea, where a strong LIW bimodality in the depth
314 domain is found (in agreement with Kokkini et al., 2019), with two peaks located at ~190 and
315 ~500 m respectively (here not shown); this behavior explains the big range that characterizes this
316 region. The investigation of the Adriatic bimodality is beyond the scope of this paper.

317

318 **3.2 Interannual variability**

319 In this section, the temporal variability of the AW and LIW in each sub-basin is studied
320 analyzing the 1-year moving average timeseries and the relative trends.

321 The results of this analysis are affected by the irregular spatial and temporal sampling of the
322 Argo floats. Time gaps in the data are found in the Catalan, Tyrrhenian and Cretan Seas (Fig. 3).
323 The missing data are both due to the lack of Argo float samplings and to the exclusion of the
324 profiles where no clear salinity peaks are found (especially during winter). Data in the Adriatic
325 Sea are available only after 2009, while the Ionian, Cretan and Levantine sub-basins have much
326 longer timeseries, with data covering the period from 2001 to 2019.

327

328 **3.2.1 Trends**

329 (i) AW trends



330 The AW salinity temporal evolution is shown in Fig. 3, where significant trends (at 5% level of
331 significance) are found in each region (Table 1). Positive trends are clearly found in the EMED,
332 highlighting a clear salinification of the AW in the last two decades over most of the
333 Mediterranean Sea ($\sim 0.007 \pm 0.021 \text{ yr}^{-1}$; Table 1). Comparable positive salinity trends between 0-
334 150 m ($\sim 0.009 \pm 0.009 \text{ yr}^{-1}$) are also found in Skliris et al. (2018) where multi-decadal salinity
335 changes in the Mediterranean Sea are investigated taking advantage of the MEDATLAS database
336 (MEDAR Group 2002) consisting of temperature and salinity profiles in the Mediterranean from
337 1945 to 2002 (<https://www.bodc.ac.uk/resources/inventories/edmed/report/4651/>). A clear
338 meridional separation between the WMED and the EMED is found in the AW trends during the
339 observed period. In the EMED the AW becomes saltier, reaching significant trends in the
340 Tyrrhenian, Adriatic, Ionian and Cretan subbasins, whilst in the WMED, a strong negative trend
341 emerges in the Algerian and Catalan subbasins (Table 1). This freshening of the AW inflow could
342 be related to the observed rapid freshening of the North Atlantic Ocean (Dickson et al. 2002),
343 which causes are related to different phenomenon, included the accelerating Greenland melting
344 triggered by the global warming (Dukhovskoy et al., 2019). These findings seem in contradiction
345 with the results provided by Millot (2007), showing a salinification of the Mediterranean inflow,
346 obtained analyzing autonomous CTDs on the Moroccan shelf in the strait of Gibraltar in the period
347 2003-2007. Nevertheless, comparing Fig. 3 in Millot (2007) and Fig. 3 in this work, a similar
348 positive trend is captured in the Algerian sub-basin, in the same period; while extending the
349 analysis to a longer timeseries, a clear negative trend leads the AW variability at interannual to
350 decadal timescale. Opposite trends are found in the EMED, where the very strong increase in net
351 evaporation of ~ 8 to 12% over 1950-2010 (Skiliris et al., 2018) and the damming of the Nile River
352 (as projected by Nof, 1979) may have caused the AW salinification. The trends are steeper in the
353 Adriatic, Ionian and Cretan sub-basins, where the salinity increases with an order of magnitude
354 higher ($O[10^{-2}]$) and the largest increase is found in the Adriatic Sea (0.051 yr^{-1}). Here the
355 impact of the negative E-P anomalies and large river runoff observed by Kokkini et al. (2019)
356 around 2014 is well captured by the salinity time series. The results in the EMED are in good
357 agreement with Fig. 9 of Kassis and Korres (2020), where the yearly average salinity per depth



358 zone and per region between 2004-2017 are shown. Similarities in the observed trend in the Ionian
359 Sea (0.012 yr^{-1}) are also found with Zu et al., 2014 (0.011 yr^{-1}), where the Argo floats data
360 between 2004 and 2014 are analyzed.

361 In contrast with the above mentioned meridional salinity transition from negative to positive
362 salinity trends moving eastward, the temperatures show a more homogeneous pattern of
363 variability, highlighting a significant increase of the AW temperature averaged over the eight
364 analyzed sub-basins ($0.018 \pm 0.026 \text{ °C/yr}$; Table 1), in agreement with a recent report from the
365 Copernicus Marine Service, showing a warming of the Sea Surface Temperature $\sim 0.04 \text{ °C/yr}$ for
366 the whole Mediterranean basin (Schuckmann et al., 2019). Interbasin changes between the
367 subbasins are instead linked to changes in the large-scale meteorological forcing of the
368 Mediterranean region (Painter and Tsimplis, 2003). As found for the salinity field, the sharper
369 increase is related to the Adriatic Sea ($\sim 0.093 \text{ °C/year}$), highlighting the presence of mechanisms
370 that enhance the trends over this region.

371 The AW depths time series (Fig. 5) show a heterogeneous trend in the Mediterranean Sea,
372 with significant negative values (the depth decreases) in the Algerian, Ionian and Levantine
373 subbasins, and positive in the Tyrrhenian and Cretan regions (Table 1), which reflects into a
374 tendency of the AW to become shallower, increasing the stratification at basin scale
375 (0.022 ± 0.216).

376

377 (ii) LIW

378 The LIW temporal variability is hereafter analyzed. Fig. 6 shows the salinity changes from
379 2001 to 2019 in the eight subbasins considered. A positive trend is found in the whole
380 Mediterranean Sea at 5% level of significance, highlighting a salinification also at intermediate
381 depths of this enclosed basin over two decades ($\sim 0.008 \pm 0.007 \text{ yr}^{-1}$; Table 1). A similar positive
382 trend between 150-600 m is found by Skliris et al. (2018), in the MEDATLAS data from 1950 to
383 2002 ($\sim 0.007 \pm 0.004 \text{ yr}^{-1}$). The LIW properties vary less than the AW as expected (about an order
384 of magnitude less), since it lies at deeper depths where air-sea interactions play a minor role. The



385 strongest salinity increase is found in the Adriatic Sea (0.025 yr^{-1}), exceeding the trends in other
386 regions by one order of magnitude.

387 The LIW salinity positive trends over the Mediterranean Sea are also found by Zu et al. (2014),
388 which confirms the salinification of the basin at intermediate depths, as also observed at surface
389 in most of the analyzed regions. This suggests that the enhancement of the net evaporation over
390 the Mediterranean in the last decades, that was observed by Skiliris et al. (2018), may lead the
391 formation of saltier LIW in the EMED, and as consequence a mean positive salinity trend over
392 the whole basin.

393 Positive temperature trends (5% level of significance) are found in the whole Mediterranean
394 Sea except in the Cretan and Levantine sub-basins where the LIW becomes colder (5% level of
395 significance; Fig. 7). This therefore highlights a zonal separation at intermediate depths in the
396 temperature trends between the Ionian Sea and the more eastward regions. By visual inspection,
397 a decadal signal overlaps the warming trend in the Cretan and Levantine sub-basins and matches
398 the low frequency signal captured by the correspondent salinity timeseries. Peaks of salinity and
399 temperature are observed in 2010 in the Levantine basin and then reach the Cretan Sea in ~ 2011 .
400 The same variability is discussed in Ozer et al. (2017) and explained in connection with the Ionian
401 Bimodal Oscillating System (BiOS). These maxima are in fact attributed to periods of
402 anticyclonic circulation in the north Ionian (2006-2009) and limited AW advection to the south-
403 eastern Levantine basin, referring to the study by Artale et al. (2006). The LIW temperature mean
404 trend and standard deviation averaged over the eight subbasins are $\sim 0.007 \pm 0.007 \text{ }^\circ\text{C/yr}$ (Table
405 1), which can be interpreted as a weaker response of the intermediate layers to the warming trend
406 observed at surface.

407 The sub-basins with the steepest increase are located in the central longitudinal band of the
408 Mediterranean Sea, therefore far from the LIW main sources. The Adriatic Sea has the larger
409 slope ($0.025 \text{ }^\circ\text{C/yr}$), followed by the Tyrrhenian ($0.009 \text{ }^\circ\text{C/yr}$) and the Ligurian, Ionian and Cretan
410 sub-basin with same mean trend ($0.006 \text{ }^\circ\text{C/yr}$). The range of temperature and salinity and the
411 respective variability in the Tyrrhenian and Ionian sub-basins are in good agreement with Poulain
412 et al. (2009), where T and S timeseries from 2001 to 2009 are computed from Argo floats data



413 near 600 m. The ranges and trends for T and S found in the Ligurian Sea are also confirmed by
414 Margirier et al. (2020), where vertical profiles collected by gliders, Argo floats, CTDs and XBTs
415 in the northwestern Mediterranean Sea over the 2007–2017 period are analyzed.

416 The LIW depth time series are shown in Fig. 8: significant negative trends (the depth
417 decreases) are found in the Tyrrhenian and Ionian Seas, while in the Adriatic and Levantine sub-
418 basins the LIW sinks ($pvalue \leq 0.05$). Non-significant trends are found in the other regions.
419 Abrupt shifts are found in the Adriatic sub-basin from ~200 m to ~500-600 m at different time
420 steps (trend ~26.397 m/yr), highlighting a bimodal behavior of the LIW depth and an intense
421 dense water production activity as also shown by Kokkini et al. (2019). Previous studies attribute
422 dramatic shifts in the Adriatic hydrological properties to the BiOS and the Eastern Mediterranean
423 Transient (e.g., Vilibić et al., 2012). This hypothesis can also be supported by correlations
424 between the BiOS (definition by Vilibić et al., 2020) and the AW/LIW salinity yearly averaged
425 timeseries in the Adriatic Sea, which maximum values are about -0.48/-0.46 at lag 0 /-4 yr (at
426 negative year lag, the BiOS leads; $pvalue \leq 0.05$). Further investigations are left to future
427 studies.

428 The results related to the EMED match those shown in Kassis and Korres (2020), where the
429 timeseries of salinity and temperature averaged between different depths-layers (below 100 m) in
430 similar subbasins are shown (see Fig. 8 in Kassis and Korres 2020). The LIW depth mean trend
431 and standard deviation averaged over the eight subbasins is 2.468 ± 9.876 m/yr (Table 1).

432

433 3.2.2 Spectral Analysis

434 The AW and LIW salinity trends confirm a salinification of the Mediterranean Sea in the last
435 two decades. The causes behind these trends are still under debate and then deserve more
436 investigations. In this section, we take a first step in this direction, analyzing the spectral features
437 of the AW and LIW salinity yearly filtered time series (Figs.3-6).

438

439 **(a) AW**



440 The wavelet power spectra show that the AW salinity (Fig. 9), during the observed periods, is
441 driven by mechanism that acts at inter-annual timescale, with significant strong peaks (magnitude
442 higher than 0.5) oscillating between 2-6 years in each subbasin. A decadal variability (*pvalue* ≤
443 0.05) emerges in the whole Mediterranean Sea, except in the Adriatic and Ionian regions, with
444 stronger energy magnitudes in the Levantine and Tyrrhenian sub-basins. It is worth to mention
445 that these results are strongly time-length dependent: the longer is the time series, the higher is
446 the probability to capture a decadal signal if present; therefore, in this respect, the Adriatic time
447 series is penalized. Similar patterns are shared by the Ligurian and Tyrrhenian regions, with a
448 high persistent peak around 3 years between the years 2005-2015; while in the Ionian and Cretan
449 sub-basins the oscillations shift in ~2009 from periods of about 5 years to higher frequencies (~2.5
450 years). In 2009, a strong peak at ~2-years is found in the Algerian, Cretan and Levantine sub-
451 basins, which overlaps a weaker decadal signal. As found in the salinity CWTs, the relative
452 patterns in the temperature domain highlight peaks between 2- and 5-years periods, while in the
453 depth domain strong peaks are centered around ~3 years in each region (not shown).

454

455 (b) LIW

456 Analyzing the LIW salinity CWTs (Fig. 10), a strong basin-dependent spectral variability
457 emerges. In this respect, in the Algerian, Ligurian, Ionian and Cretan sub-basins, the salinity is
458 mainly led by oscillations around 3-years, while in the Catalan, Tyrrhenian and Adriatic Seas the
459 period of the oscillations increases reaching ~5-8- years. Decadal oscillations dominate the
460 salinity variability in the Levantine region. In order to better investigate the decadal variability,
461 longer time series are needed.

462 A significant energy peak is found in the Algerian sub-basin before 2011 at period of ~2.5-3
463 years, which is also present in the Ligurian, Ionian and Cretan sub-basin in the next years.

464 Comparing the salinity CWTs for the AW and LIW in each sub-basin, other features emerge.
465 Strong differences appear in the Ligurian, Tyrrhenian, Ionian, Cretan and Levantine sub-basins:
466 in the Ligurian, Ionian and Cretan Seas, the low-frequency variability observed in the AW
467 disappears at intermediate depths, while in the Tyrrhenian and Levantine Seas the LIW does not



468 show high-frequency oscillations with period of ~2-3 years, suggesting that the AW is much more
469 non-stationary compared to the LIW. In fact, lying at deeper depths, it is less modulated by
470 external forcings (the seasonality, the air-sea interactions and the freshwater fluxes play a minor
471 role).

472

473 **4 Conclusions**

474 We presented an analysis of the main properties and variability of the AW and LIW in the
475 Mediterranean Sea, exploiting the Argo float data that provide an optimal observational dataset
476 to study their thermohaline properties. Indeed, this dataset covers the water column down to
477 ~2000 m and provide data for almost two decades.

478 Taking advantage of different diagnostics discussed in section 2, the AW and LIW have been
479 detected in the Mediterranean Sea through a sub-basin approach, which allowed to define the
480 main hydrological features over this enclosed basin in different regions.

481 In addition to previous studies, this work provides a more detailed view of the AW and LIW
482 characteristics in the last two-decades over most of the Mediterranean Sea, except for the Alboran
483 sub-basin, the Sicily Channel and the Aegean sub-basin where Argo data are too scarce.

484 To achieve this goal, the first step of this study was the detection of the AW and LIW cores in
485 each available profile. In agreement with previous studies, we confirmed the zonal gradients of
486 the AW and LIW properties over the Mediterranean Sea: the AW becomes saltier, warmer, denser
487 and deeper moving eastward, while the LIW becomes less salty, colder, denser and deeper moving
488 westward. These results not only match the present literature but also provide a more detailed
489 view of these water masses over eight sub-basins.

490 The timeseries derived from the AW and LIW parameters have also highlighted some
491 interesting features that are in good agreement with the previous literature. The most relevant
492 results are summarized below:

- 493 • Positive salinity and temperature trends characterize the AW and LIW in the last two
494 decades over most of the Mediterranean Sea (average value over the whole region:
495 0.007 and 0.008 yr⁻¹; 0.018 and 0.007 °C/yr respectively). The warming and



496 salinification of the Mediterranean Sea is in good agreement with previous results
497 (e.g., Skliris et al., 2018; Margirier et al., 2020; Kassis and Korres, 2020).

498 • Negative AW salinity trends in the Algerian and Catalan sub-basins suggest a
499 freshening of the AW inflow, in agreement with the observed rapid freshening of the
500 North Atlantic Ocean (Dickson et al., 2002).

501 • Positive AW salinity trends are found east of the Catalan sub-basin, highlighting a
502 clear salinification of this water mass in the last two decades probably due to the
503 combined effect of the strong increase in net evaporation and the Nile dumping (e.g.,
504 Nof, 1979; Skliris et al., 2018; section 3.2.1a).

505 • Positive trends in the LIW salinity timeseries are found in the whole Mediterranean
506 Sea at 5% level of significance, highlighting a salinification also at intermediate
507 depths (section 3.2.1b).

508 • Positive LIW temperature trends ($pvalue \leq 0.05$) are found everywhere except in the
509 Cretan and Levantine sub-basins where the LIW becomes colder ($pvalue \leq 0.05$).
510 This highlights a meridional separation at intermediate depths in the temperature
511 trends between the Ionian Sea and the more eastward regions.

512 • The AW and LIW depth trends are highly space-dependent, showing different
513 behaviors in the eight sub-basins.

514 • The steepest trends are found in the Adriatic Sea in both the AW and LIW and for
515 each variable (Table 1). The AW temperature increases 0.093 °C/yr, while the LIW
516 temperature shows a trend about 0.059 °C/yr. Abrupt shifts are found in the Adriatic
517 sub-basin from ~200 m to ~500-600 m at different time steps (trend ~24.671 m/yr),
518 highlighting a bimodal behavior of the LIW depth and an intense dense water
519 production activity as also shown by Kokkini et al. (2019).

520 These results therefore provide interesting new insights about the AW and LIW interbasin and
521 interannual variability, which can be further analyzed to investigate which mechanisms lead to
522 the observed temporal trends in each sub-basin. A preliminary attempt in this direction is provided
523 by the spectral analysis of the filtered salinity timeseries (without seasonal variability). Peaks



524 between 2.5-6 years are found in the whole Mediterranean Sea in the AW salinity, and hints of
525 decadal variability appear everywhere, except in the Ionian and Adriatic regions. A strong basin-
526 dependent spectral variability emerges in the LIW salinity timeseries. In this respect, in the
527 Algerian, Ligurian, Ionian and Cretan sub-basins, the salinity is mainly characterized by
528 oscillations with a period around 3-years, while in the Catalan, Tyrrhenian and Adriatic Seas the
529 period of the oscillations increases to ~5-8- years. Decadal oscillations dominate the salinity
530 variability in the Levantine region, that could be related to the BIOS as suggested by Ozer et al.
531 (2017). In order to investigate the decadal oscillations, longer timeseries are needed. Finally,
532 comparing the AW and LIW salinity CWTs we find that the AW is much more non-stationary
533 compared to the LIW since flowing in the surface layer, it can be modulated by more external
534 forcings. Further studies on the leading mechanisms over each subbasin are left for future
535 investigations.



536 **References**

537

538 Argo: Argo float data and metadata from Global Data Assembly Centre (Argo GDAC). SEANOE.

539 <https://doi.org/10.17882/42182>, 2020.

540

541 Artale V., Calmante S., Malanotte-Rizzoli P., Pisacane G., Rupolo V., and Tsimplis M., In:
542 Lionello, P., Malanotte-Rizzoli, P., Boscoli, R. (Eds.), *The Atlantic and Mediterranean Sea*
543 as connected systems, in *Mediterranean Climate Variability Dev. Earth Environ. Sci.* 4.
544 Elsevier, Amsterdam, pp. 283–323, 2006.

545

546 Azzaro M., La Ferla R., Maimone G., Monticelli L.S., Zaccone R., and Civitarese G.: Prokaryotic
547 dynamics and heterotrophic metabolism in a deep convection site of Eastern Mediterranean
548 Sea (the Southern Adriatic Pit), *Continental Shelf Research*, Volume 44 2012, Pages 106-118,
549 ISSN 0278-4343, <https://doi.org/10.1016/j.csr.2011.07.011>, 2012.

550

551 Bensi M., Cardin V., Rubino A., Notarstefano G., and Poulain P.M.: Effects of winter convection
552 on the deep layer of the Southern Adriatic Sea in 2012, *J. Geophys. Res. Oceans*
553 118, 6064– 6075, <https://doi.org/10.1002/2013JC009432>, 2013.

554

555 Berkowitz J., and Kilian L.: Recent developments in bootstrapping time series. *Econometr Rev*
556 19:1–48, <https://doi.org/10.1080/07474930008800457>, 2000.

557

558 Bergamasco, A., and Malanotte-Rizzoli P.: The circulation of the Mediterranean Sea: A historical
559 review of experimental investigations. *Adv. Oceanogr. Limnol.* 2010 1 11–28;
560 <https://doi.org/10.1080/19475721.2010.491656>, 2010.

561

562 Borghini M., Bryden H., Schroeder K., Sparnocchia S., and Vetrano A.: The Mediterranean is
563 becoming saltier, *Ocean Sci.* 10, 693–700, <https://doi.org/10.5194/os-10-693-2014>, 2014.



564

565 Bosse A., Testor P., Mortier L., Prieur L., Taillandier V., d'Ortenzio F., and Coppola L.:
566 Spreading of Levantine Intermediate Waters by submesoscale coherent vortices in the
567 northwestern Mediterranean Sea as observed with gliders. *Journal of Geophysical Research.*
568 *Oceans*, Wiley-Blackwell 2015 120 (3), pp.1599-1622,
569 <https://doi.org/10.1002/2014JC010263>, 2015.

570

571 Bethoux J.P., Gentili B., Raunet J., and Taillez D.: Warming trend in the Western Mediterranean
572 deep water. *Nature* 347, 660–662, <https://doi.org/10.1038/347660a0>, 1990.

573

574 Cabanes C., Thierry V., and Lagadec C.: Improvement of bias detection in Argo float conductivity
575 sensors and its application in the North Atlantic. *Deep Sea Research Part I: Oceanographic*
576 *Research Papers* 114 128-136, <https://doi.org/10.1016/j.dsr.2016.05.007>, 2016.

577

578 Conraria L.A., and Soares M.J.: The continuous wavelet transform: a primer. NIPE WP.
579 <http://www3.eeg.uminh o.pt/economia/nipe/>, 2011.

580

581 Demirov E. K., and Pinarci N.: On the relationship between the water mass pathways and eddy
582 variability in the Western Mediterranean Sea, *J. Geophys. Res.* 112, C02024,
583 <https://doi.org/10.1029/2005JC003174>, 2007.

584

585 Dickson B., Yashayaev I., Meincke J., Turrell B., Dye S., and Holfort J.: Rapid freshening of the
586 deep North Atlantic Ocean over the past four decades. *Nature* 416, 832–837,
587 <https://doi.org/10.1038/416832a>, 2002.

588

589 Dukhovskoy D.S., Yashayaev I., Proshutinsky A., Bamber J. L., Bashmachnikov I.
590 L., Chassignet E. P., Lee C.M., and Tedstone A.J.: Role of Greenland freshwater anomaly in



591 the recent freshening of the subpolar North Atlantic. *Journal of Geophysical Research:*
592 *Oceans*, 124, 3333–3360. <https://doi.org/10.1029/2018JC014686>, 2019.

593

594 Escudier R., Mourre B., Juza M., and Tintoré J.: Subsurface circulation and mesoscale variability
595 in the Algerian subbasin from altimeter-derived eddy trajectories, *J. Geophys. Res. Oceans*
596 121, 6310–6322, <https://doi.org/10.1002/2016JC011760>, 2016.

597

598 Font J., Millot C., Pérez JDJS, Julià A., and Chic O.: The drift of Modified Atlantic Water from
599 the Alboran Sea to the eastern Mediterranean. *Scientia Marina*. 62. 211-216,
600 <https://doi.org/10.3989/scimar.1998.62n3211>, 1998.

601

602 Giorgi F.: Climate change hot-spots. *Geophysical Research Letters*, 33: L08707,
603 <https://doi.org/10.1029/2006GL025734>, 2006.

604

605 Hayes D. R., Schroeder K., Poulain P.M., Testor P., Mortier L., Bosse, A., Du Madron X.: Review
606 of the Circulation and Characteristics of Intermediate Water Masses of the
607 Mediterranean: Implications for Cold-Water Coral Habitats. In: Orejas C., Jiménez C.
608 (eds) *Mediterranean Cold-Water Corals: Past, Present and Future*. Coral Reefs of the
609 World, vol 9. Springer, Cham, https://doi.org/10.1007/978-3-319-91608-8_18, 2019.

610

611 Hernández-Molina F., Stow D., Zarikian C., Acton G., Bahr A., Balestra B., Ducassou E., Flood
612 R., Flores J.A., Furota S., Grunert P., Hodell D., Jiménez-Espejo F., Kim J.K., Krissek L.,
613 Kuroda J., Li B., Llave E., Lofi J., and Xuan C.: Onset of Mediterranean outflow into the North
614 Atlantic. *Science*. 344, <https://doi.org/10.1126/science.1251306>, 2014.

615



- 616 Kassis D., and Korres G.: Hydrography of the Eastern Mediterranean basin derived from argo
617 floats profile data, *Deep Sea Research Part II: Topical Studies in Oceanography*, Volume
618 171,2020,104712,ISSN 0967-0645, <https://doi.org/10.1016/j.dsr2.2019.104712>, 2020.
619
- 620 Kokkini Z., Mauri M., Gerin R., Poulain P.M., Simoncelli S., and Notarstefano G.: On the salinity
621 structure in the South Adriatic as derived from float and glider observations in 2013–2016,
622 *Deep Sea Research Part II: Topical Studies in Oceanography*, Volume 171 2020 104625, ISSN
623 0967-0645, <https://doi.org/10.1016/j.dsr2.2019.07.013>, 2019.
624
- 625 Kubin E., Poulain P.M, Mauri E., Menna M., and Notarstefano G.: Levantine Intermediate and
626 Levantine Deep Water Formation: An Argo Float Study from 2001 to 2017,
627 <https://doi.org/10.3390/w11091781>, 2019.
628
- 629 Kreyszig E.: *Introductory Mathematical Statistics: Principles and Methods*. New York: Wiley,
630 1970.
631
- 632 Lamer P.A., Mauri E., Notarstefano G., and Poulain P.M.: The Levantine Intermediate Water in
633 the eastern Mediterranean Sea; http://maos.inogs.it/pub/REPORT_LAMER_final_last.pdf,
634 2019.
635
- 636 Lascaratos A., Williams R.G., and Tragou E.: A mixed-layer study of the formation of Levantine
637 intermediate water. *Journal of Geophysical Research* 98, <https://doi.org/10.1029/93JC00912>,
638 1993.
639
- 640 Lipizer, M., Partescano, E., Rabitti, A., Giorgetti, A., and Crise, A.: Qualified temperature,
641 salinity and dissolved oxygen climatologies in a changing Adriatic Sea, *Ocean Sci.*, 10, 771–
642 797, <https://doi.org/10.5194/os-10-771-2014>, 2014.
643



644 Malanotte-Rizzoli P., Manca B., Marullo S., Ribera d'Alcala M., Roether W., Theocharis A.,
645 Bergamasco A., Budillon G., Sansone E., Civitarese G., Conversano F., Gertman I., Hernt B,
646 Kress N., Kioroglou S., Kontoyiannis H., Nittis K., Klein B., Lascaratos A., and Kovacevic
647 V.: The Levantine Intermediate Water Experiment (LIWEX) Group: Levantine basin—A
648 laboratory for multiple water mass formation processes. *Journal of Geophysical Research*. 108.
649 8101, <https://doi.org/10.1029/2002JC001643>, 2003.

650

651 Mauri E., Sitz L., Gerin R., Poulain P.M., Hayes D., and Gildor H.: On the Variability of the
652 Circulation and Water Mass Properties in the Eastern Levantine Sea between September 2016–
653 August 2017. *Water* **2019**, *11*, 1741, <https://doi.org/10.3390/w11091741>, 2019.

654 Mauri, E., Menna, M., Garić, R., Batistić, M., Libralato, S., Notarstefano, G., Martellucci, R.,
655 Gerin, R., Pirro, A., Hure, M., Poulain, P-M, 2021. Recent changes of the salinity distribution
656 and zooplankton community in the South Adriatic Pit, accepted in OSR5.

657 Margirier F., Testor P., Heslop E., Mallil K., Bosse A., Houpert L., Mortier L., Bouin M.-
658 N., Coppola L., D'Ortenzio F., de Madron X.D., Mourre B., Prieur L., Raimbault P., and
659 Taillandier V.: Abrupt warming and salinification of intermediate waters interplays with
660 decline of deep convection in the Northwestern Mediterranean Sea. *Sci Rep* 10 20923,
661 <https://doi.org/10.1038/s41598-020-77859-5>, 2020.

662

663 Millot C., and Taupier-Letage I.: Circulation in the Mediterranean Sea: Updated description and
664 schemas of the circulation of the water masses in the whole Mediterranean Sea. A. Saliot. *The*
665 *Mediterranean Sea, The Mediterranean Sea (5-K)*, Springer, pp.29-66 2005, *Handbook of*
666 *Environmental Chemistry*, 9783540314929 9783540250180.ff10.1007/b107143ff. fihal-
667 01191856v1f, <https://doi.org/10.1007/b107143>, 2005.

668



669 Millot C., Candela J., Fuda J.L., and Tber Y.: Large warming and salinification of the
670 Mediterranean outflow due to changes in its composition. *Deep-Sea Res.* 53, 656–665,
671 <https://doi.org/10.1016/j.dsr.2005.12.017>, 2006.

672

673 Millot C.: Interannual salinification of the Mediterranean inflow, *Geophys. Res. Lett.*, 34,
674 L21609, doi:10.1029/2007GL031179, 2007.

675

676 Millot C.: Levantine Intermediate Water characteristics: An astounding general
677 misunderstanding. *Scientia Marina*. 78, <https://doi.org/10.3989/scimar.04045.30H>, 2013.

678

679 Millot C.: Levantine intermediate water characteristics: an astounding general misunderstanding!
680 (addendum). *Sci. Marina*, 78 165-171, <https://doi.org/10.3989/scimar.04045.30H>, 2014.

681

682 Nof D.: On man-induced variations in the circulation of the Mediterranean Sea. *Tellus* 31, 558–
683 564, 1979.

684

685 Notarstefano G., and Poulain P. M.: Delayed mode quality control of Argo floats salinity data in
686 the Tyrrhenian Sea. Technical Report OGS 2008/125 OGA 43 SIRE,
687 http://nettuno.ogs.trieste.it/sire/DMQC/dmqc_1900593_54073_V1.pdf, 2008.

688



689 Notarstefano G., and Poulain P. M.: Thermohaline variability in the Mediterranean and Black
690 Seas as observed by Argo floats in 2000–2009. OGS Tech. Rep. OGS 2009/121 OGA 26 SIRE,
691 72 pp.-171, <http://dx.doi.org/10.3989/scimar.04045.30H>, 2009.

692

693 Notarstefano G., and Poulain P.M.: Delayed mode quality control of Argo salinity data in the
694 Mediterranean Sea: A regional approach. Technical Report OGS 2013/103 Sez. OCE 40
695 MAOS, 2013.

696

697 Ozer T., Gertman I., Kress N., Silverman J., and Herut B.: Interannual thermohaline (1979–2014)
698 and nutrient (2002–2014) dynamics in the Levantine surface and intermediate water masses,
699 SE Mediterranean Sea. *Global and Planetary Change*, 151, 60–67.
700 [doi:10.1016/j.gloplacha.2016.04.001](https://doi.org/10.1016/j.gloplacha.2016.04.001), 2017.

701

702 Painter S.C., and Tsimplis M.N.: Temperature and salinity trends in the upper waters of the
703 Mediterranean Sea as determined from the MEDATLAS dataset, *Continental Shelf Research*,
704 Volume 23, Issue 16 2003, Pages 1507-1522, ISSN 0278-4343,
705 <https://doi.org/10.1016/j.csr.2003.08.008>, 2003.

706

707 Poulain P.M., Barbanti R., Font J., Cruzado A., Millot C., Gertman I., Griffa A., Molcard A.,
708 Rupolo V., Le Bras S., and Petit de la Villeon L.: MedArgo: a drifting profiler program in the
709 Mediterranean Sea. *Ocean Science*, European Geosciences Union 2007, 3 (3), pp.379- 395.
710 hal-00331145, <https://doi.org/10.5194/osd-3-1901-2006>, 2007.

711



712 Poulain P.M., Solari M., Notarstefano G., and Rupolo V.: Assessment of the Argo sampling in
713 the Mediterranean and Black Seas (part II).
714 http://maos.inogs.it/pub/2009_report_task4.4_partII.pdf, 2009.

715

716 Rahmstorf S.: Thermohaline Ocean Circulation. In: Encyclopedia of Quaternary Sciences, Edited
717 by S. A. Elias. Elsevier, Amsterdam, [http://www.pik-](http://www.pik-potsdam.de/~stefan/Publications/Book_chapters/rahmstorf_eqs_2006.pdf)
718 [potsdam.de/~stefan/Publications/Book_chapters/rahmstorf_eqs_2006.pdf](http://www.pik-potsdam.de/~stefan/Publications/Book_chapters/rahmstorf_eqs_2006.pdf), 2006.

719

720 Roemmich D., Johnson G., Riser S., Davis R., Gilson J., Owens W., Garzoli S., Schmid C., and
721 Mark I.: The Argo Program Observing the Global Ocean with Profiling Floats. *Oceanography*.
722 22, <https://doi.org/10.5670/oceanog.2009.36>, 2009.

723

724 Rohling E.J., and Bryden H.L.: Man induced salinity and temperature increase in the Western
725 Mediterranean Deep Water. *J. Geophys. Res.* 97 (C7) 11191–11198,
726 <https://doi.org/10.1029/92JC00767>, 1992.

727

728 Rubino A., Gačić M., Bensi M., Vedrana K., Vlado M., Milena M., Negretti M.E., Sommeria J.,
729 Zanchettin D., Barreto R.V., Ursella L., Cardin V., Civitarese G., Orlic M., Petelin B., and
730 Siena G.: Experimental evidence of long-term oceanic circulation reversals without wind
731 influence in the North Ionian Sea. *Sci Rep* 10 1905 (2020), [https://doi.org/10.1038/s41598-](https://doi.org/10.1038/s41598-020-57862-6)
732 [020-57862-6](https://doi.org/10.1038/s41598-020-57862-6), 2020.

733

734 Schroeder K., Chiggiato J., Josey S., Borghini M., Aracri S., and Sparnocchia S.: Rapid response
735 to climate change in a marginal sea. *Scientific Reports*. 7, [https://doi.org/10.1038/s41598-017-](https://doi.org/10.1038/s41598-017-04455-5)
736 [04455-5](https://doi.org/10.1038/s41598-017-04455-5), 2017.

737



- 738 Schroeder K.,: Current Systems in the Mediterranean Sea, Editor(s): J. Kirk Cochran, Henry J.
739 Bokuniewicz, Patricia L. Yager, Encyclopedia of Ocean Sciences (Third Edition), Academic
740 Press 2019, Pages 219-227, ISBN 9780128130827, [https://doi.org/10.1016/B978-0-12-](https://doi.org/10.1016/B978-0-12-409548-9.11296-5)
741 [409548-9.11296-5](https://doi.org/10.1016/B978-0-12-409548-9.11296-5), 2019.
742
- 743 Shaltout M., and Omstedt A.: Recent sea surface temperature trends and future scenarios for the
744 Mediterranean Sea, *Oceanologia*, Volume 56, Issue 3 2014, Pages 411-443, ISSN 0078-3234,
745 <https://doi.org/10.5697/oc.56-3.411>, 2014.
746
- 747 Schuckmann K.V., Traon P.-Y.L., Smith N., Pascual A., Djavidnia S., Gattuso J.-P., Grégoire M.,
748 Nolan G., Aaboe S., Aguiar E., et al.: Copernicus marine service ocean state report, issue 3. *J.*
749 *Oper. Oceanogr.*, 12, S1–S123, 2019.
750
- 751 Skliris N.: Past, Present and Future Patterns of the Thermohaline Circulation and Characteristic
752 Water Masses of the Mediterranean Sea. In: Goffredo S., Dubinsky Z. (eds) *The*
753 *Mediterranean Sea*. Springer, Dordrecht, https://doi.org/10.1007/978-94-007-6704-1_3, 2014.
754
- 755 Skliris N., Zika J.D., Herold L., Josey S.A., and Marsh R.: Mediterranean sea water budget long-
756 term trend inferred from salinity observations. *Clim Dyn* **51** 2857–2876 (2018).
757 <https://doi.org/10.1007/s00382-017-4053-7>, 2018.
758
- 759 Tsimplis M., Zervakis V., Josey S.A., Peneva E., Struglia M.V., Stanev E., Lionello P.,
760 Malanotte-Rizzoli P., Artale V., Theocharis A., Tragou E., and Oguz T.: Changes in the
761 oceanography of the Mediterranean Sea and their link to climate variability. In: Lionello, P.;
762 Malanotte-Rizzoli, P.; and Boscolo, R., (eds.) *Mediterranean climate variability*. Amsterdam,
763 The Netherlands, Elsevier 227-282, 438pp. (Developments in Earth and Environmental
764 Sciences, 4), [https://doi.org/10.1016/S1571-9197\(06\)80007-8](https://doi.org/10.1016/S1571-9197(06)80007-8), 2006.
765



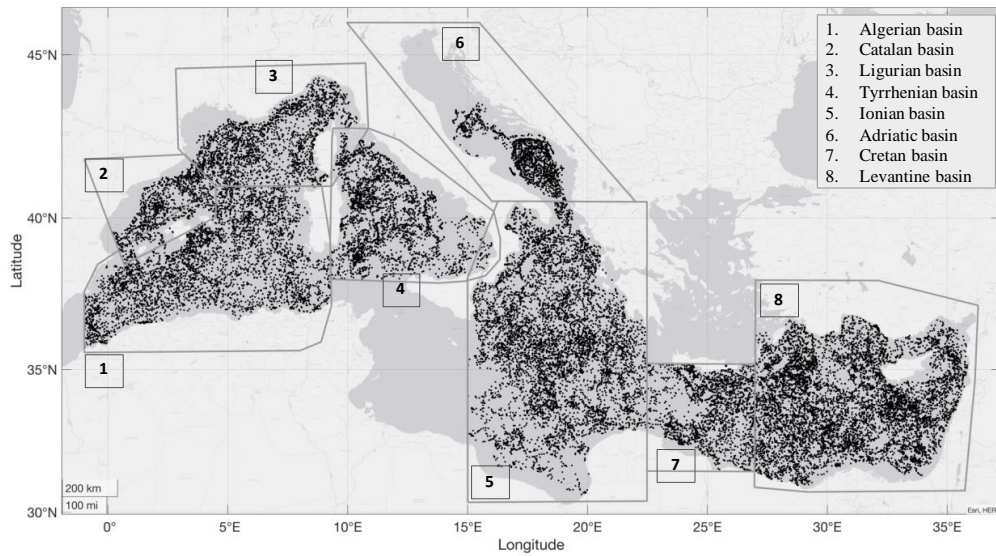
- 766 Vargas-Yáñez M., Moya F., Tel E., García-Martínez M.C., Guerber E., and Bourgeon M.:
767 Warming and salting of the Western Mediterranean during the second half of the XX century:
768 inconsistencies, unknowns and the effect of data processing. *Sci. Mar.* 73 (1), 7–28,
769 <https://doi.org/10.3989/scimar.2009.73n1007>, 2009.
- 770
- 771 Vargas-Yáñez M., Moya F., García-Martínez M.C., Tel E., Zunino P., Plaza F., Salat J., Pascual
772 J., López-Jurado J.L., and Serra M.: Climate change in the Western Mediterranean Sea 1900–
773 2008, *Journal of Marine Systems*, Volume 82, Issue 3 2010, Pages 171-176, ISSN 0924-7963,
774 <https://doi.org/10.1016/j.jmarsys.2010.04.013>, 2010.
- 775
- 776 Wong A., Keeley R., Carval T., Argo Data Management Team: Argo Quality Control Manual for
777 CTD and Trajectory Data, <https://doi.org/10.13155/33951>, 2021.
- 778
- 779 Zu Z., Poulain P.M., and Notarstefano G.: Changes in hydrological properties of the
780 Mediterranean Sea over the last 40 years with focus on the Levantine Intermediate Water and
781 the Atlantic Water, http://maos.inogs.it/pub/Hydro_trend_LIW_SAW_core_report_v10.pdf,
782 2014.
- 783



Table 1. Trends by year for the AW and LIW salinity (S), temperature (T) and depth (D) timeseries in eight Mediterranean subbasins. In bold characters the trends significant at 5% level. The rightmost column shows the mean and standard deviation trend values computed over the eight subbasins.

TREND (S) l/yr	Algerian subbasin	Catalan subbasin	Ligurian subbasin	Tyrrhenian subbasin	Adriatic subbasin	Ionian subbasin	Cretan subbasin	Levantine subbasin	Mean±Std
AW	-0.021	-0.004	-0.000	0.007	0.051	0.012	0.011	0.003	0.007 ± 0.021
LIW	0.003	0.003	0.006	0.009	0.025	0.006	0.006	0.002	0.008±0.007
TREND (T) °C/yr									
AW	0.067	0.037	0.005	0.039	0.093	0.028	-0.024	0.033	0.018±0.026
LIW	0.017	0.013	0.024	0.037	0.059	0.027	-0.012	-0.024	0.007±0.007
TREND (D) m/yr									
AW	-0.135	-0.001	0.090	0.256	0.055	-0.277	0.361	-0.170	0.022±0.216
LIW	-0.176	0.317	0.248	-5.630	24.671	-2.415	-0.426	1.213	2.225±9.323

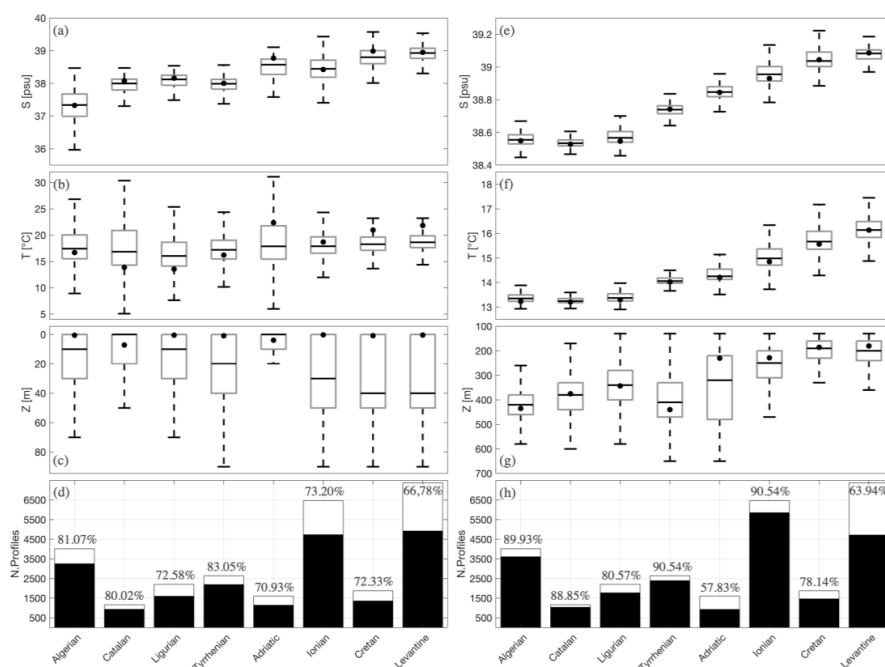
784



785

786 Fig. 1 Argo floats profiles scatter plot in the Mediterranean Sea between 2001 and 2019 in eight

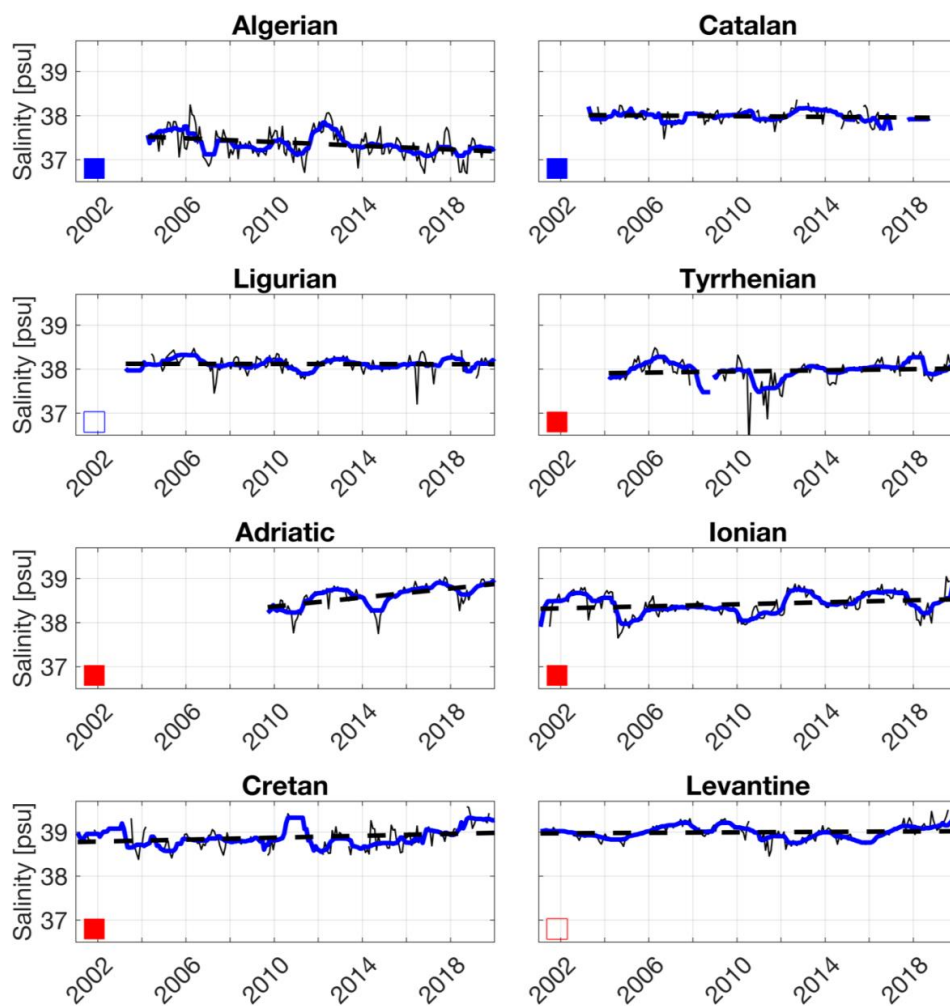
787 regions based on the climatological areas defined by the EU/MEDARMEDATLAS II project.



788

789 Fig. 2 Boxplot diagrams for the AW salinity (a), temperature (b) and depth (c) in eight
 790 Mediterranean subbasins. The number of effective profiles (black bars) for each, compared with
 791 the total profiles (white bars) are shown in panel (d). The numbers indicate the percentages of
 792 effective profiles related to the total number available in each subbasin. The corresponding
 793 diagrams for the LIW are shown in the panels (e,f,g,h).

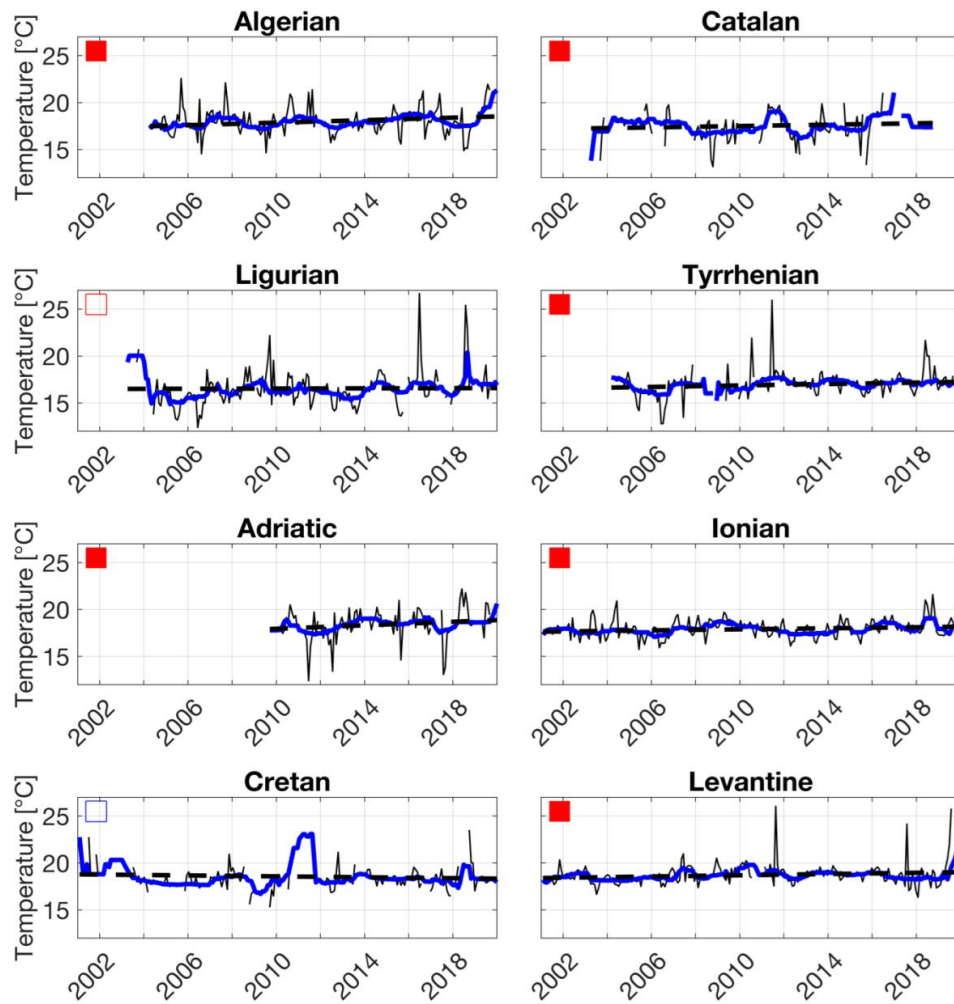
794



795

796 Fig. 3 AW salinity timeseries in eight subbasins: the thin black lines show the monthly timeseries
797 (seasonal cycle filtered out), the thick blue lines are the 1-year moving average timeseries and the
798 dashed black lines are the trends. The red/blue filled squares identify the positive/negative trends
799 with $p\text{-value} \leq 0.05$, while the red/blue not-filled squares identify the positive/negative trends with
800 $p\text{-value} > 0.05$.

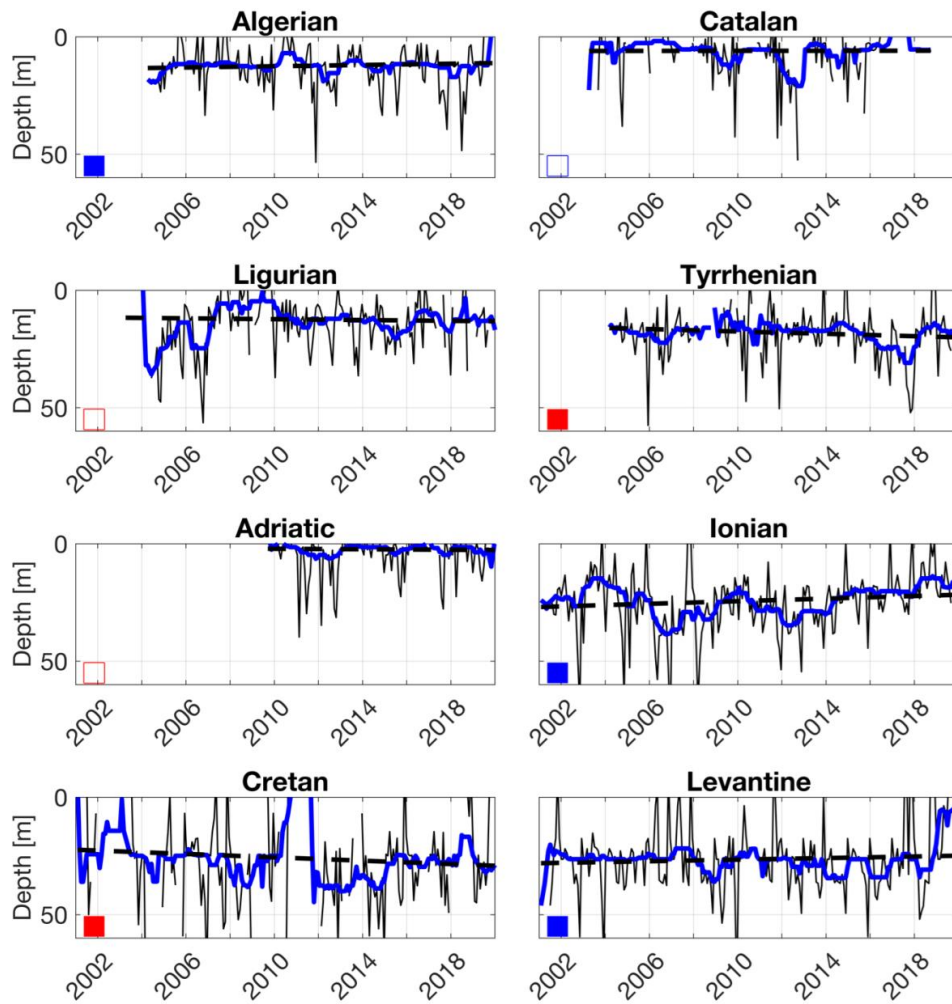
801



802

803 Fig. 4 Same as Fig. 3 but for the AW temperature.

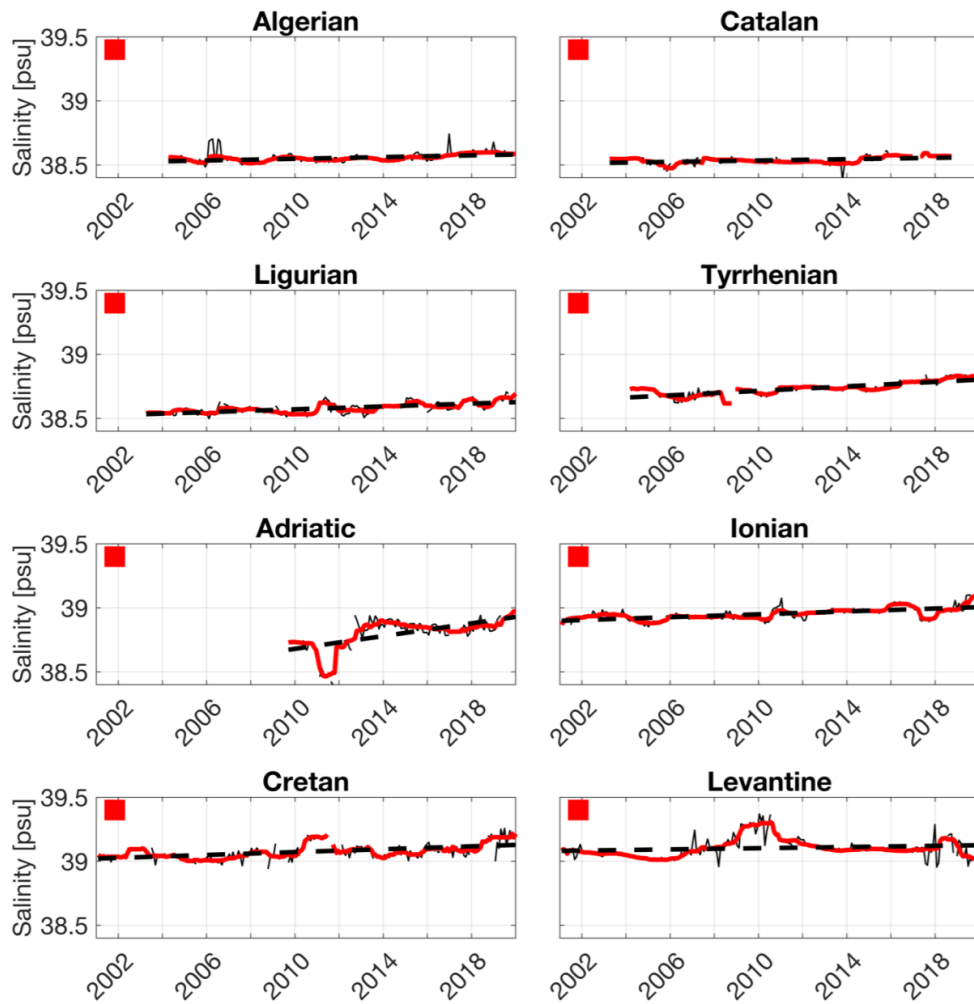
804



805

806 Fig. 5 Same as Fig. 3 but for the AW depth.

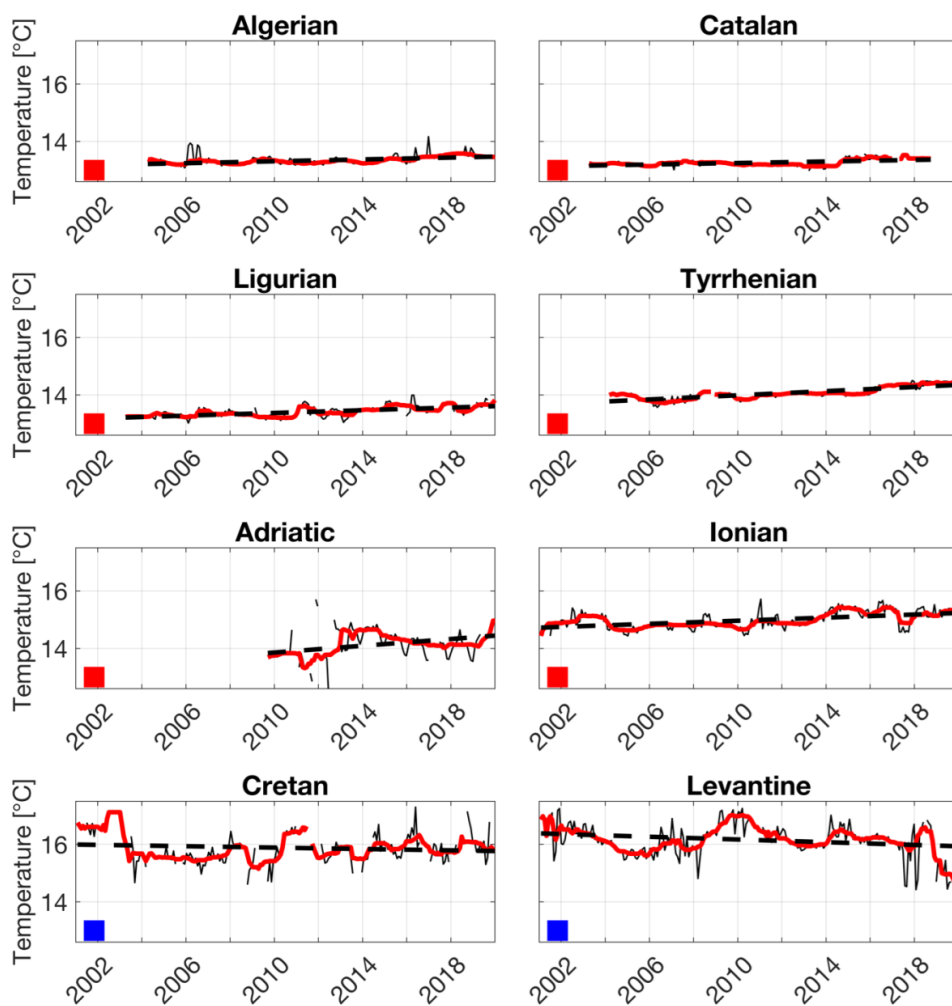
807



808

809 Fig. 6 Same as Fig. 3 but for the LIW salinity.

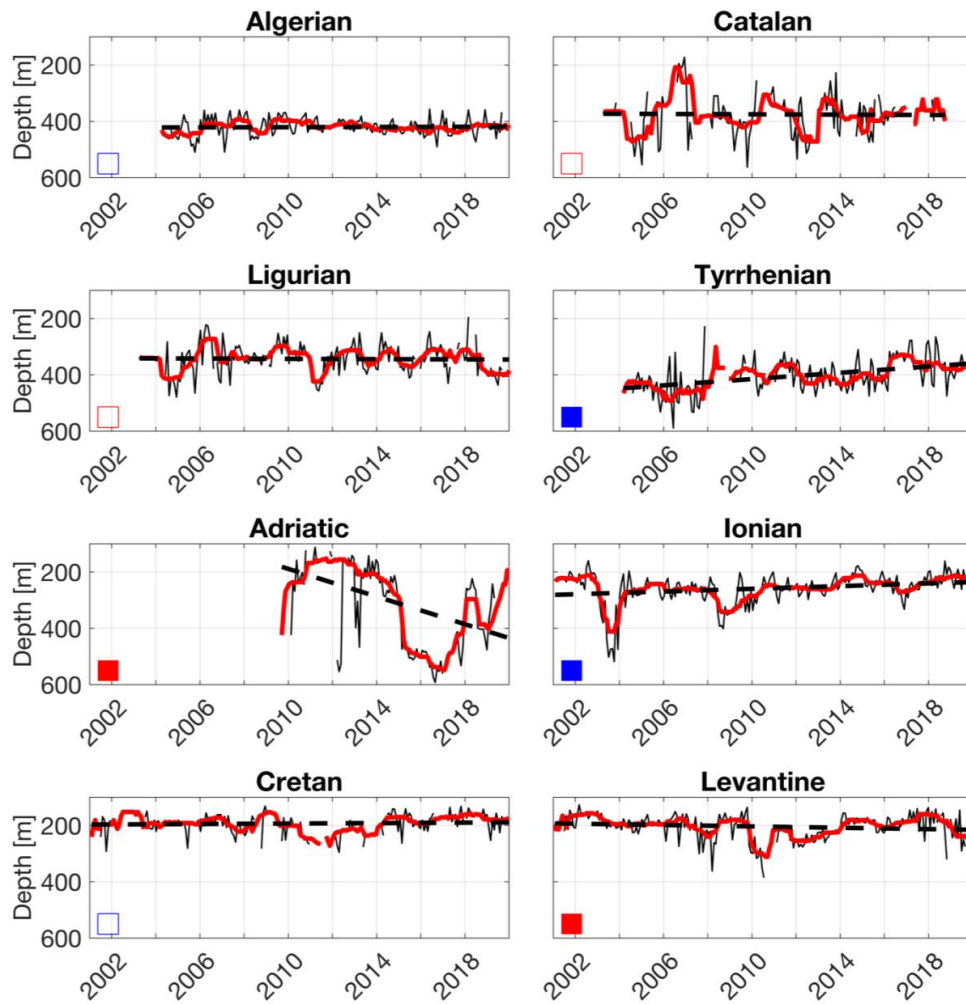
810



811

812 Fig. 7 Same as Fig. 3 but for the LIW temperature.

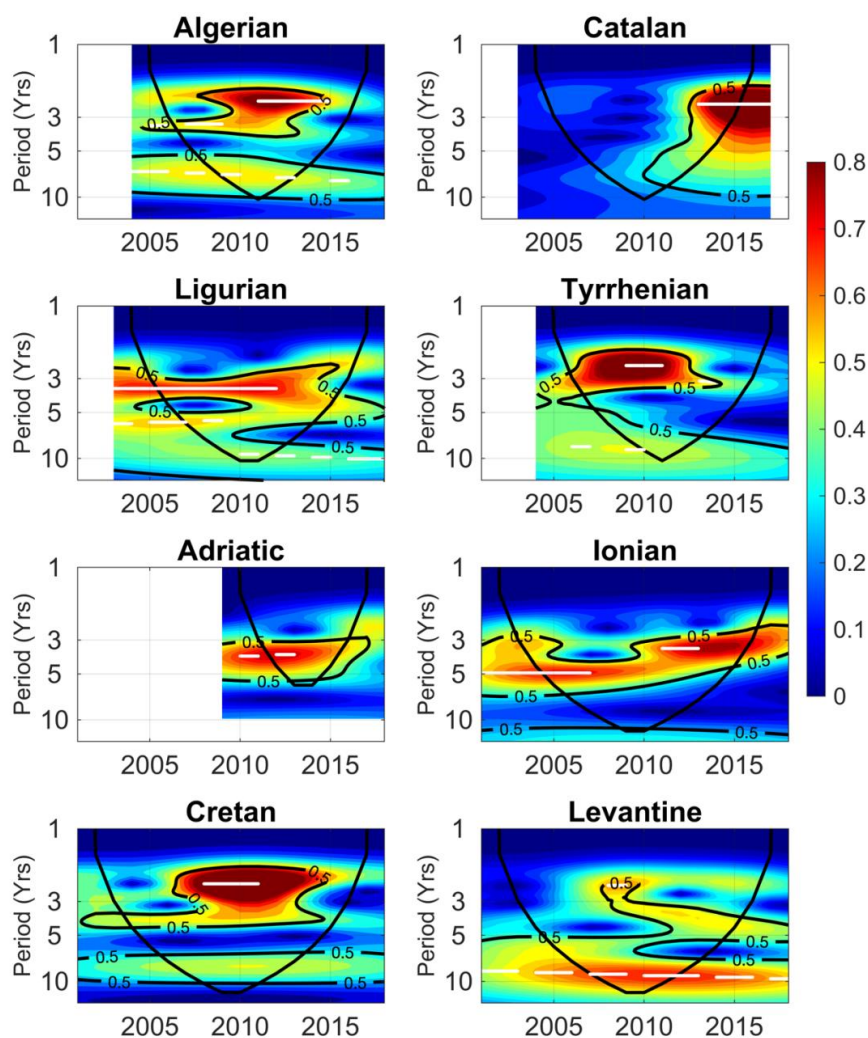
813



814

815 Fig. 8 Same as Fig. 3 but for the LIW depth.

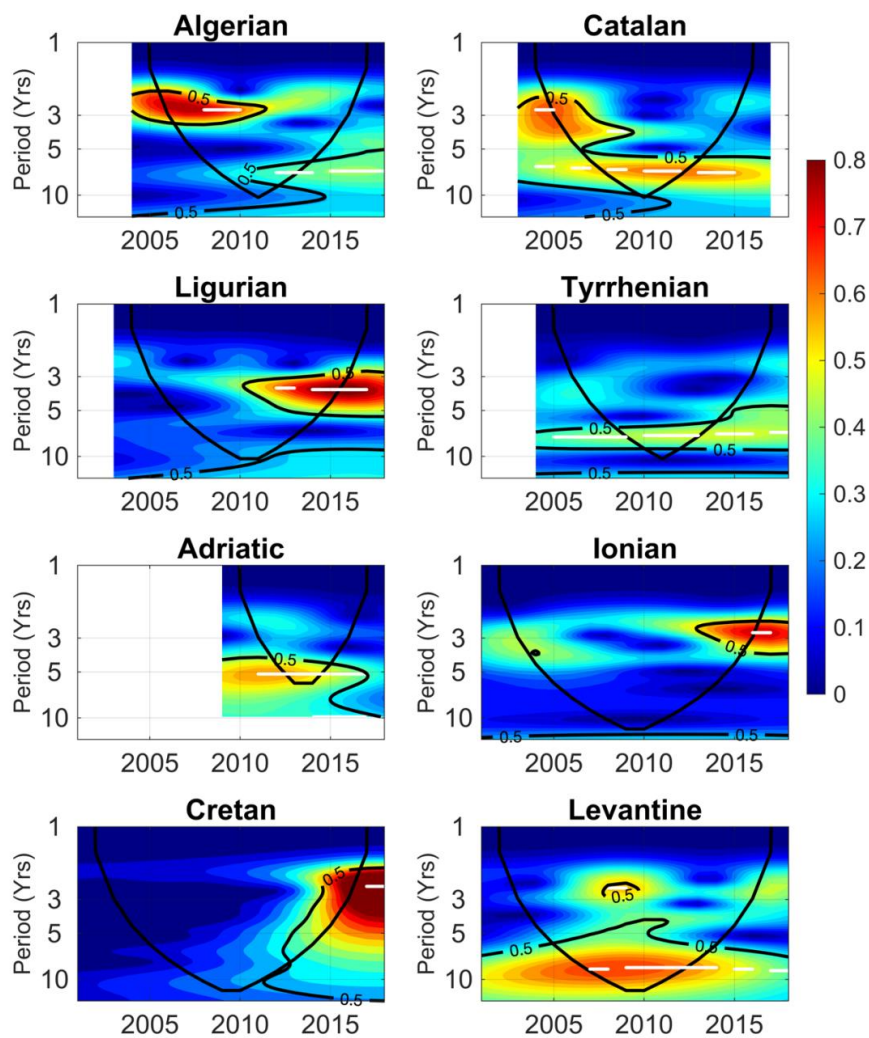
816



817

818 Fig. 9 Wavelet power spectra of the low-pass filtered AW salinity for the eight subbasins
819 considered. The black contour designates the 5% significance level based on Monte Carlo
820 simulations (Berkowitz and Kilian, 2000). The cone of influence, which indicates the region
821 affected by edge effects, is shown with a thick black line. The color code for power ranges from
822 blue (low power) to red (high power). The white lines show the main ridges of the wavelet power
823 spectrum.

824



825

826 Fig. 10 Same as Fig. 9 but for the LIW salinity.